

Pixel-based inverse lithography using a mask filtering technique

Wen Lv^a, Qi Xia^b, and Shiyuan Liu^{*, a, b}

^a Wuhan National Laboratory for Optoelectronics, Huazhong University of Science and Technology, Wuhan 430074, China;

^b State Key Laboratory of Digital Manufacturing Equipment and Technology, Huazhong University of Science and Technology, Wuhan 430074, China.

ABSTRACT

In this paper, we propose a new regularization framework that regularizes mask directly by applying a mask filtering technique to improve computational efficiency and enhance mask manufacturability for pixel-based Inverse Lithography Technique (ILT). Generally, the synthesized mask by pixel-based ILT is a grey-level image, and possesses small, unwanted block objects, such as isolated holes, protrusions, and jagged edges, which are unreachable in the real manufacturing process. The proposed method filters (or regularizes) mask directly to guarantee manufacturability of the synthesized mask pattern; this technique is different from the conventional regularization method that regularizes mask by incorporating various penalty functions to a cost function. A tailored mask filter is developed in this special ILT case. In addition, we introduce a new metric, edge distance error which has the same dimension nanometer as edge placement error and has a continuous expression as pattern error, to guide mask synthesis. Simulation results demonstrating the validity and efficiency of the proposed method are presented.

Keywords: Inverse Lithography Technology (ILT), computational efficiency, manufacturability, regularization, mask filtering technique, edge distance error (EDE)

1. INTRODUCTION

Inverse Lithography Technology (ILT), as one of resolution enhancement techniques (RETs)^[1, 2], is considered as an economically viable method to meet various challenges in the future technology nodes. Pixel-based ILT considers a mask as a raster image constituted by pixels and synthesizes it pixel-by-pixel^[3]. It is probably the most popular ILT in the literature due to its high flexibility and ease of understanding and implementation. Generally, pixel-based ILT treats mask synthesis as a rigorous inverse mathematical problem that aims at minimizing a cost function on the difference between the output and desired mask patterns^[3]. However, the synthesized mask by pixel-based ILT is usually a grey-level image, and possesses small, unwanted block objects, such as isolated holes, protrusions, and jagged edges, which are unreachable in the real manufacturing process^[3-6]. To address these problems, regularization approaches are introduced to guarantee the synthesized mask to be binary and less complex. In the literature, almost all the regularization approaches take the regularization terms as penalty functions incorporated into the cost function with corresponding weighted parameters^[3-8] as

$$F\{M\} = \|\Gamma\{M\} - Z^*\|_2^2 + \sum_{k=1}^K \lambda_k R_k(M). \quad (1)$$

Here, the operator $\Gamma\{\cdot\}$ is the forward mapping from the input mask M to the output pattern, Z^* is the desired output pattern, $R_k(M)$ are the various regularization terms. Generally, regularization terms can be classified into two types: one is related to the manufacturability, such as quadratic penalty term^[3], total variation penalty term^[3], and wavelet penalty term^[5]; the other one is related to the fabrication process, such as image slope term and mask error enhancement factor (MEEF)^[7, 8]. λ_k is the weight of the corresponding regularization term $R_k(M)$. It should be noted that λ_k plays a critical role in the optimization process, however, how and why to choose a λ_k are rarely discussed in the literature. It is usually set as a constant by experience in advance. Here, we take the quadratic penalty term as an example to illustrate how weighted parameter λ impacts the optimization process. In this case, both smaller pattern error and quadratic error are preferred, where the pattern error is calculated by $\|\Gamma\{M\} - Z^*\|_2^2$ and the quadratic error is equal to the value of

* Corresponding author: shyliu@mail.hust.edu.cn; phone: +86 27 87559543; webpage: <http://www2.hust.edu.cn/nom>.

quadratic penalty term $R(M)$ [3]. As Fig. 1 shows, a smaller weighted parameter λ of the quadratic penalty term results in a rapid convergence on pattern error. It is observed from Fig. 1(a) that the pattern error may meet the requirement after 44 iterations, while the quadratic error is pretty high at this moment; it still needs extra iterations to reduce the quadratic error. On the other hand, a larger λ results in a good performance on the quadratic error while causing a poor convergence on the pattern error, as Fig. 1(d) reveals. As we can see from Fig. 1, the convergence of the pattern error and the quadratic error under such a regularization framework is out of synchronization. Noticing that a smaller λ will not achieve the regularization effects while a larger λ may result in a larger pattern error, it is therefore difficult to choose an appropriate constant value of λ . Moreover, the choosing of λ has a close relation with the mask features and simulation resolution. In mathematics, a solid approach is that the λ is adaptive in each iteration. However, this in turn increases the freedom of design variable, and it is generally tough to accomplish.

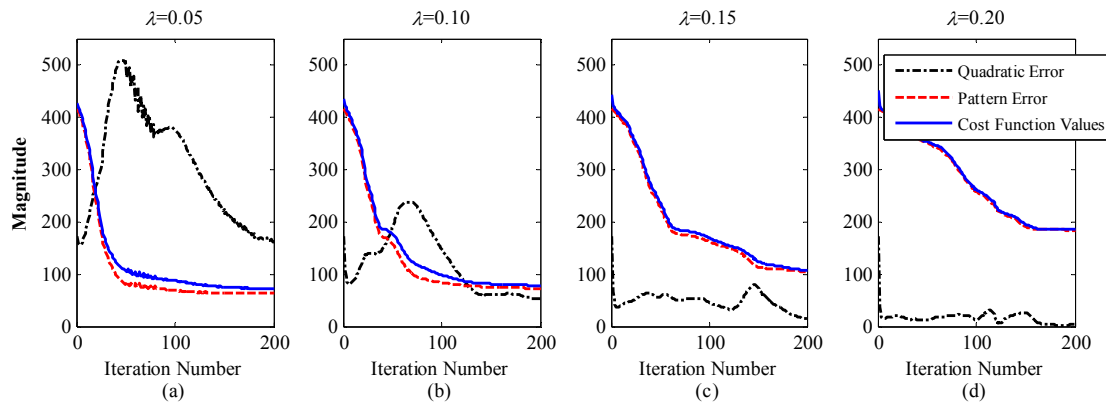


Fig. 1. The convergence of pattern error, quadratic error and cost function values with different weighted parameters λ of quadratic penalty term, both using the mask M^1 in Fig. 8 under the corresponding illumination condition.

In this paper, we propose a new regularization framework that regularizes the mask directly by using a mask filtering technique. In such a framework, the original cost function Eq. (1) is changed to Eq. (2) as

$$F\{M\} = \|\Gamma\{S[M]\} - Z^*\|_2^2, \quad (2)$$

where $S[\cdot]$ is a mask filtering operator, and it is designed based on the manufacturing constraints. It is noted that the pattern error $F\{M\}$ of the filtered mask $S[M]$ instead of the original mask M , is calculated and will be iteratively reduced in the optimization process. The filtering technique is widely used in signal and image processing, and has been used for many years in various application fields as a numerical method to ensure regularity or existence of solutions to an engineering problem, such as structural topology optimization problem [9, 10]. In this paper, grey-level transitions and small, unwanted block objects in the mask are all interpreted as unwanted noises, and it is therefore natural to use filters to remove these noises to satisfy the manufacturing constraints. Section 2.3 details this mask filtering technique.

Moreover, we introduce a new metric, edge distance error (EDE), to guide mask synthesis in the ILT framework. It has the same dimension nanometer as edge placement error (EPE) but has a continuous expression as pattern error. The detailed description of EDE will be given in Section 2.2.

In addition, with the critical dimension (CD) decreasing, the printed dimension becomes increasingly sensitive to the fluctuation in the fabrication process, which limits the yield in the semiconductor industry. Instead of using process penalty terms, such as image slope term and MEEF, a statistical strategy is applied to minimize the exception of EDE under different process variations weighted by their statistical probability to enhance the robustness of layout patterns [12-14]. This approach is directly related to the fabrication process and is well understood and easily accomplished, while using process penalty terms can be considered as a roundabout regularization approach and requires deeper understanding of mask topology and the imaging system.

The remainder of this paper is organized as follows. Section 2 details the proposed mask filtering technique. Section 3 provides the simulation results to demonstrate the validity and efficiency of the proposed method. Finally, we draw some conclusions in Section 4.

2. METHODOLOGY

2.1 The lithography imaging model

Abstractly, the imaging process for optical lithography is mathematically described as

$$Z(\mathbf{r}) = \Gamma\{M(\mathbf{r})\}, \quad (3)$$

where \mathbf{r} represents spatial coordinates (x, y) , and the operator $\Gamma\{\cdot\}$ is the forward mapping from the input mask $M(\mathbf{r})$ to the output pattern $Z(\mathbf{r})$. In practice, the $\Gamma\{\cdot\}$ in Eq. (3) consists of projection optics effect and resist effect. The projection optics effect, namely the optical image in resist $I(\mathbf{r})$, can be modeled as a pupil function with a partially coherent illumination source^[15], which can be approximated by the sum of coherent systems (SOCS) method^[11], the optimal coherent approximation (OCA) approach^[16], or the analytical circle-sampling technique^[17] as the superposition of several coherent systems,

$$I(\mathbf{r}) = \sum_{q=1}^n \lambda_q |h_q(\mathbf{r}) \otimes M(\mathbf{r})|^2. \quad (4)$$

Here $h_q(\mathbf{r})$ is the q^{th} optical kernel, λ_q is the eigenvalue of the q^{th} kernel with n kernels in total, and \otimes denotes the 2-D convolution. The resist effect can be approximated by a constant threshold resist (CTR) model using a logarithmic Sigmoid function^[3],

$$\text{sig}(I(\mathbf{r})) = \frac{1}{1 + e^{-a(I(\mathbf{r})-t)}}, \quad (5)$$

with a being the steepness of the Sigmoid function and t being the threshold. In reality, t is equal to the threshold level of the resist. Combining Eqs. (4) and (5), we can write the lithography imaging equation as

$$Z(\mathbf{r}) = \Gamma\{M(\mathbf{r})\} = \text{sig}(I(\mathbf{r})) = \text{sig}\left(\sum_{q=1}^n \lambda_q |h_q(\mathbf{r}) \otimes M(\mathbf{r})|^2\right). \quad (6)$$

2.2 Edge distance error and the inverse lithography problem definition

Generally, L_2 norm is employed as a metric to evaluate the difference between the output pattern of $M(\mathbf{r})$ and the desired pattern $Z^*(\mathbf{r})$ in pixel-based ILT framework as

$$F\{M(\mathbf{r})\} = \|\Gamma\{M(\mathbf{r})\} - Z^*(\mathbf{r})\|_2. \quad (7)$$

$F\{M\}$ is called pattern error. It is noted that pattern error is a continuous function, and hence the gradient of $F\{M\}$ with respect to the mask can be analytically calculated^[3, 6]. However, this metric is not intuitive, for its magnitude is not directly related to the CD error and highly depends on the mask features and simulation parameters, such as simulation grid size. To address this problem, we therefore introduce a derivation from the pattern error, which can convey CD information and is independent of mask features and simulation parameters. In Fig. 2, the red dots are discrete pixels of resist; S_{shadow} denotes the absolute area between the target contour and the real resist contour, and L is the perimeter of the target feature. The edge distance error (EDE) is defined as

$$\text{EDE} = \frac{S_{\text{shadow}}}{L}. \quad (8)$$

It is noted that the EDE has the same dimension of nanometer as EPE. It can be interpreted as the mean EPE when segments are small enough. Assuming the pixel grid size is small enough, S_{shadow} can be approximated by multiplying the total number of pixels in shadow by the element (pixel) area as

$$S_{\text{shadow}} = N \cdot (\delta_x \cdot \delta_y). \quad (9)$$

It is noted that N is the total number of the red dots in the shadow as Fig. 2 shows. Since the value of pixel in resist is either 0 or 1, according to the definition of pattern error in Eq. (7), the N is almost equal to pattern error, namely, $N = F\{M\}$. Substituting $N = F\{M\}$ into Eq. (9) and then into Eq. (8), the EDE can be approximated by $G(M)$ as

$$\text{EDE} \cong G(M) = \frac{S_{\text{shadow}}}{L} = \frac{(\delta_x \cdot \delta_y)}{L} \cdot F\{M\}. \quad (10)$$

In this paper, we adopt $G(M)$ to express and calculate the EDE.

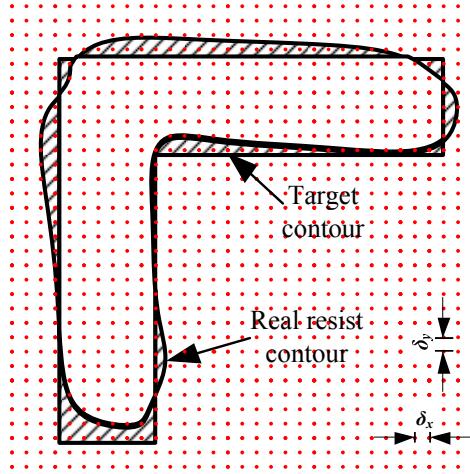


Fig. 2. The pixel-based expression theory of resist.

Generally, $G(M)$ is treated as a cost function to guide mask synthesis under nominal conditions, i.e., no defocus or dosage variations, *etc.* In order to enhance process robustness, process variations should be taken into account under the mask synthesizing process. Here, we use the expectation of EDE under different variations as a cost function as expressed by

$$J(M) = \zeta[\psi(\mathbf{var}) \cdot G(M; \mathbf{var})], \quad (11)$$

where ζ denotes expectation, \mathbf{var} represents a collection of parameters of process variations including, for example, defocus, exposure dosage variation, and lens aberrations, *etc.*, and $\psi(\mathbf{var})$ is the statistical probability of the process variation \mathbf{var} . $J(M)$ is called the statistical EDE and is used as a cost function to guide the mask synthesis. The gradient of $J(M)$ with respect to mask M will be used in the optimization process, and it is given as

$$\begin{aligned} \nabla_M J = & \sum_{\mathbf{var}} a \cdot \frac{(\delta_x \cdot \delta_y)}{L_w} \cdot \psi(\mathbf{var}) \cdot \left\{ \sum_{q=1}^n \lambda_q h_q^{\text{flip}}(\mathbf{r}; \mathbf{var}) \otimes [(Z - Z^*) \cdot Z \cdot (\mathbf{1} - Z) \cdot (h_q^\dagger(\mathbf{r}; \mathbf{var}) \otimes M)] \right\} \\ & + \sum_{\mathbf{var}} a \cdot \frac{(\delta_x \cdot \delta_y)}{L_w} \cdot \psi(\mathbf{var}) \cdot \left\{ \sum_{q=1}^n (\lambda_q h_q^{\text{flip}}(\mathbf{r}; \mathbf{var}))^\dagger \otimes [(Z - Z^*) \cdot Z \cdot (\mathbf{1} - Z) \cdot (h_q(\mathbf{r}; \mathbf{var}) \otimes M)] \right\}, \end{aligned} \quad (12)$$

where \dagger means the conjugate operator; $h_q(\mathbf{r}; \mathbf{var})$ is the q^{th} optical kernel under the process variation \mathbf{var} ; $h_q^{\text{flip}}(\mathbf{r}; \mathbf{var})$ is the up-down and left-right flip of $h_q(\mathbf{r}; \mathbf{var})$, i.e., $h_q^{\text{flip}}(\mathbf{r}; \mathbf{var})|_{i,j} = h_q(\mathbf{r}; \mathbf{var})|_{N-i+1, N-j+1}$, where i, j are integers and belong to $[1, N]$; and a is the steepness of the Sigmoid function in Eq. (5).

In order to guarantee mask manufacturability, mask quadratic error and complexity should be considered. In this paper, the quadratic metric $R_Q(M)$ and the complexity metric $R_{\text{TV}}(M)$ [3] are adopted to quantify the corresponding performance. In this paper, we focus on the binary mask. So the quadratic metric $R_Q(M)$ and the complexity metric $R_{\text{TV}}(M)$ [3] are expressed respectively as:

$$R_Q(M) = \int_{\Omega} [1 - (2M - 1)^2] d\mathbf{r}, \quad (13)$$

$$R_{\text{TV}}(M) = \left\| \frac{\partial M}{\partial x} \right\|_1 + \left\| \frac{\partial M}{\partial y} \right\|_1 = \|DM\|_1 + \|MD^T\|_1, \quad (14)$$

where Ω is the simulation area, or the number of pixels in M , $\|\cdot\|_1$ is L_1 norm and D is an operator of first derivative as

$$D = \begin{bmatrix} 1 & -1 & & & 0 \\ & 1 & -1 & & \\ & & \ddots & \ddots & \\ & & & 1 & -1 \\ 0 & & & -1 & 1 \end{bmatrix}. \quad (15)$$

Therefore, combining the optimization objectives of mask quadratic metric, mask complexity, and the statistical EDE, we state the inverse lithography problem as:

$$\begin{aligned} & \text{Finding } M^*(\mathbf{r}) \text{ to minimize: } J(M), R_Q(M) \text{ and } R_{TV}(M) \\ & \text{subject to: } 0 \leq M \leq 1. \end{aligned}$$

It is noted that this problem has three mutually exclusive minimization objectives. In the literature, they are usually combined with certain proportions λ_1 and λ_2 to state a single-objective minimization problem^[3-6] as:

$$\begin{aligned} & \text{Finding } M^*(\mathbf{r}) \text{ to minimize: } J(M) + \lambda_1 R_Q(M) + \lambda_2 R_{TV}(M) \\ & \text{where: } \lambda_1, \lambda_2 \geq 0 \\ & \text{subject to: } 0 \leq M \leq 1. \end{aligned}$$

2.3 The mask filtering technique

In this paper, we propose an alternative method to solve this multiple-objective minimization problem. We first interpret grey-level transitions and small, unwanted block objects, such as isolated holes, protrusions, and jagged edges or other details that cannot be fabricated, as unwanted noises in the mask, and then design a tailored filter $S[\cdot]$ to remove these noises to satisfy manufacturing constraints,

$$\tilde{M} = S[M]. \quad (16)$$

After the filtering process, the quadratic metric $R_Q(M)$ and complexity metric $R_{TV}(M)$ of the filtered mask \tilde{M} are rather small. Then we calculate the statistical EDE of this filtered mask,

$$J(M) = \zeta [\psi(\mathbf{var}) \cdot G(S[M]; \mathbf{var})]. \quad (17)$$

In the optimization process, we ensure that the statistical EDE of the filtered mask is iteratively decreasing. It should be noted that the synthesized mask after each iteration is filtered and satisfies all the optimization objectives except the statistical EDE; namely, it satisfies the manufacturing constraints. As a result, we only need to reduce the statistical EDE of this filtered mask. In this perspective, the multiple-objective minimization problem is degraded to a single-objective minimization problem. This approach is called the mask filtering technique. The filter operator $S[\cdot]$ is very flexible, for it can be defined based on different mask manufacturing rules. This makes it possible for the filtered mask to be sent to fabrication directly. The most basic filter should filter the gray-level image to be a district 0 or 1 and guarantee mask to be less complex. In this paper, we therefore define a basic mask filter as

$$S[M] = \text{sig}[\tau^{-1} \cdot (O \otimes M)]. \quad (18)$$

Here, the steepness of this Sigmoid function is a_s and the threshold is t_s , O is a Gauss filter to relieve mask complexity,

$$O(\mathbf{r}) = e^{-(1/2)(\|\mathbf{r}-\mathbf{r}_0\|/\sigma_0)^2}, \quad (19)$$

where \mathbf{r}_0 is the center point and $\|\mathbf{r}-\mathbf{r}_0\|$ means the distance from \mathbf{r} to \mathbf{r}_0 . τ is the normalized weight of the Gauss filter $O(\mathbf{r})$,

$$\tau = \int_{\Omega_1} O(\mathbf{r}) d\mathbf{r}, \quad (20)$$

where Ω_1 is the number of pixels in $O(\mathbf{r})$. The gradient of $S[\cdot]$ with respect to M is given as

$$\nabla_M S[M] = \tau^{-1} \cdot O^{flip} \otimes \left\{ a_s \cdot \text{sig}[\tau^{-1} \cdot (O \otimes M)] \cdot [\mathbf{1} - \text{sig}[\tau^{-1} \cdot (O \otimes M)]] \right\}. \quad (21)$$

Combining Eqs. (12) and (21), the gradient of $J(M)$ with respect to M is,

$$\nabla_M J = \frac{\partial J}{\partial S} \frac{\partial S}{\partial M} = \nabla_S J \cdot \nabla_M S. \quad (22)$$

With the gradient Eq. (22), we apply a steep-descent method^[3] to solve this problem.

3. SIMULATIONS

Simulations were performed on a partially coherent imaging system with an annual source illumination whose outer radius was $\sigma_{\text{out}} = 0.7$ and whose inner radius was $\sigma_{\text{in}} = 0.4$. The wavelength in the simulations was set to be 193nm, and the numerical aperture (NA) was 1.35. The maximum optical image of a single bar with target CD was normalized to 1. The resist effects were approximated by a Sigmoid function with $a = 100$ and $t = 0.7$. The Gauss filter $O(\mathbf{r})$ has a size of 21×21 pixels and $\sigma_O = 4$. The parameters of the Sigmoid function in the proposed filter $S[\cdot]$ were $a_S = 300$ and $t_S = 0.5$. Since we focus on developing a new regularization framework in this paper, process variations will not be taken into consideration in the proposed simulations. That means \mathbf{var} is the nominal process condition and therefore $\psi(\mathbf{var}) = 1$. All the simulations were carried out on a HPZ800 workstation of 3.47 GHz Xeon.

3.1 Simulations of edge distance error

An example of a real resist feature and a target pattern is presented in Fig. (3). In this case, the true absolute area between the target contour and the real resist contour is $1.853 \times 10^4 \text{nm}^2$, the perimeter of the target pattern is $1.70 \times 10^3 \text{nm}$, and therefore the true EDE is 10.90nm. Table 1 summarizes the relative error compared to the true EDE when using different pixel grid size. The EDE in Table 1 is calculated by Eq. (10) and the pattern error is calculated by Eq. (7). From Table 1, it is observed that the magnitude of pattern error varies with the pixel grid size while the EDE does not. When the pixel grid size is small enough (0.5nm for example), the EDE calculated by the proposed method is almost equal to the true value. With the increase of pixel grid size, the accuracy of the EDE remains acceptable. So the EDE calculated by the proposed method can be used to guide mask synthesis.

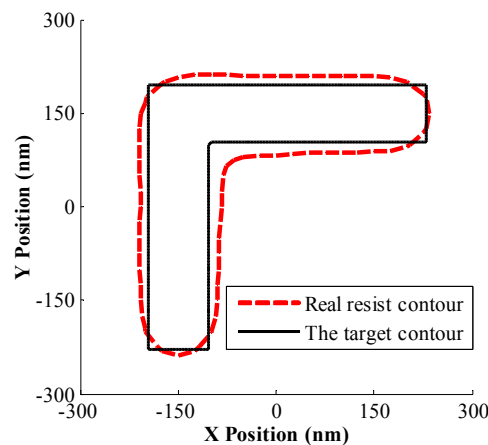


Fig. 3. Comparison of the real resist contour and the target contour.

Table 1. Results of the pattern error and the EDE when using different pixel grid size.

Pixel grid size (nm)	0.5	1	1.5	2.5	3
EDE (nm)	10.897	10.768	10.610	10.352	10.124
Pattern Error	7.410×10^5	1.831×10^5	8.017×10^4	2.816×10^4	1.912×10^4
Relative EDE error	0.28%	1.2%	2.7%	5.0%	7.1%

3.2 Simulations of the mask filtering technique

Figure 4 shows the performance of the proposed method with a common circuit pattern SRAM. All images are of size 321×321 pixels with a grid resolution of 2.5 nm. The target CD is 45nm. The optimization is terminated after 200 iterations. M^* is the desired SRAM pattern, and $\Gamma(M^*)$ is its output binary pattern on the wafer with an EDE of 10.48nm.

M^S is the mask obtained by the proposed method, and $\Gamma(M^S)$ is its output pattern with an EDE of 1.28nm. M^P is the absolute binary mask, which is obtained by a post-processing of M^S using a global threshold 0.5, and $\Gamma(M^P)$ is its output pattern with an EDE of 1.28nm. $I(\cdot)$ is the corresponding optical image of the input mask M . It is observed that the synthesized grey-mask M^S is very close to the post-processing mask M^P , and reaches an almost identical resist feature and EDE.

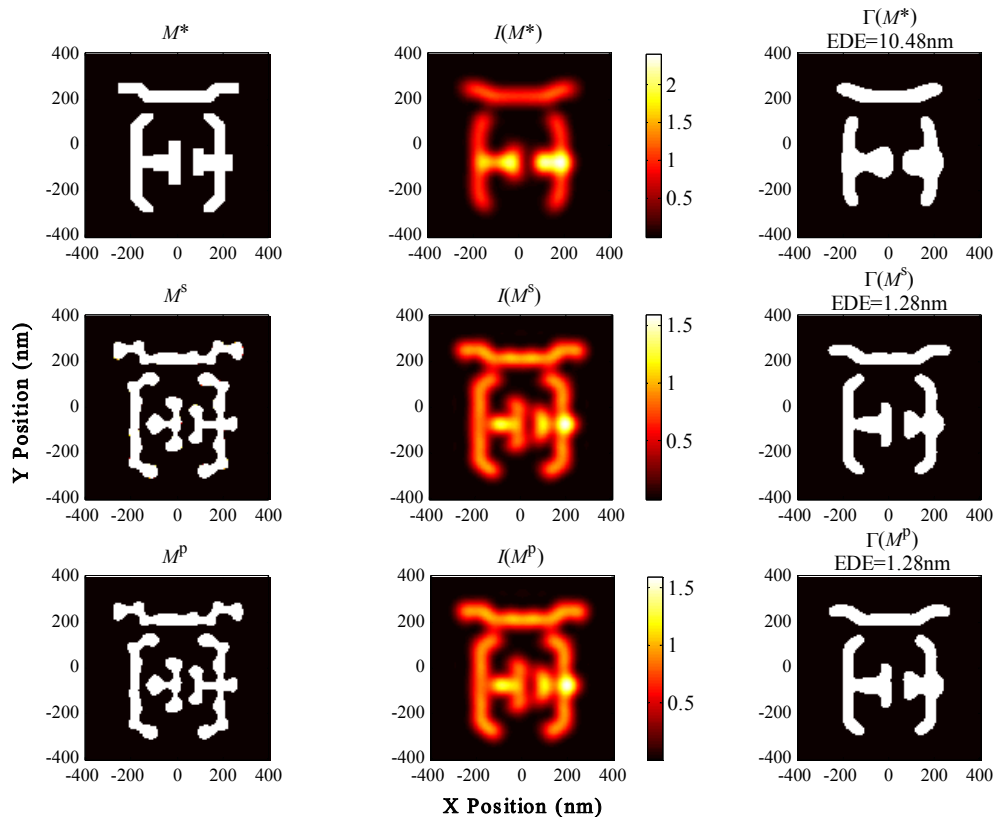


Fig. 4. Simulation results of the proposed method. M^* is the target mask, M^S is the synthesized mask by the proposed method, M^P is the binary mask which is obtained by a post-processing of M^S using a global threshold 0.5, $I(\cdot)$ is corresponding optical image in resist and $\Gamma(\cdot)$ represents the resist features.

Figure 5 presents some intermediate results obtained in the iteration process by the proposed method. $M\#0$ denotes the initial mask; $M\#n$ means mask that is obtained after the n -th iteration. The EDE means the EDE between the resist feature of the $M\#n$ and the target pattern. It is noted that each obtained intermediate mask is very close to binary and has a low mask complexity. This demonstrates that the proposed method can regularize the mask to eliminate the grey-level transitions and small, unwanted objects.

Figure 6 presents some intermediate results obtained in the iteration process by the conventional regularization method. The conventional regularization method takes different penalty terms and incorporates them into the cost function with the corresponding weight, and then seeks the minimum of such a weighted cost function. In this case, we take the quadratic term, and the corresponding weighted parameter λ is set to be 0.1. From Fig. 6, it is observed that the intermediate result with this method possesses grey-level transitions. The EDE may satisfy a 5%CD error after 50 iterations, while the quadratic error is pretty high at this moment; it still needs extra iterations to reduce the quadratic error, although the EDE achieves the demand. This is one of the drawbacks of the conventional regularization method.

As revealed in Fig. 5 and Fig. 6, the intermediate mask with the proposed method has a low level in quadratic error and mask complexity, which is quite an improvement over the conventional regularization method. Since the convergence of the EDE and the quadratic error with the conventional regularization method is out of synchronization, it therefore needs several iterations to achieve a low level on both the EDE and the quadratic error. With the proposed method, the iteration

(optimizing process) can be stopped whenever the EDE reaches the demand without worrying about the manufacturability. What's more, compared to the conventional regularization method, the proposed method does not raise computational complexity; it just adds a computation of Eq. (21) whose runtime is far less than the total calculation time. In this simulation case, the average runtime of each iteration with the proposed method is 1.183s, while the one with the conventional regularization method is 1.175s. That means the proposed method enhances the mask manufacturability with an almost equal runtime compared to the conventional regularization method. In this perspective, the proposed method is therefore more efficient than the conventional regularization method.

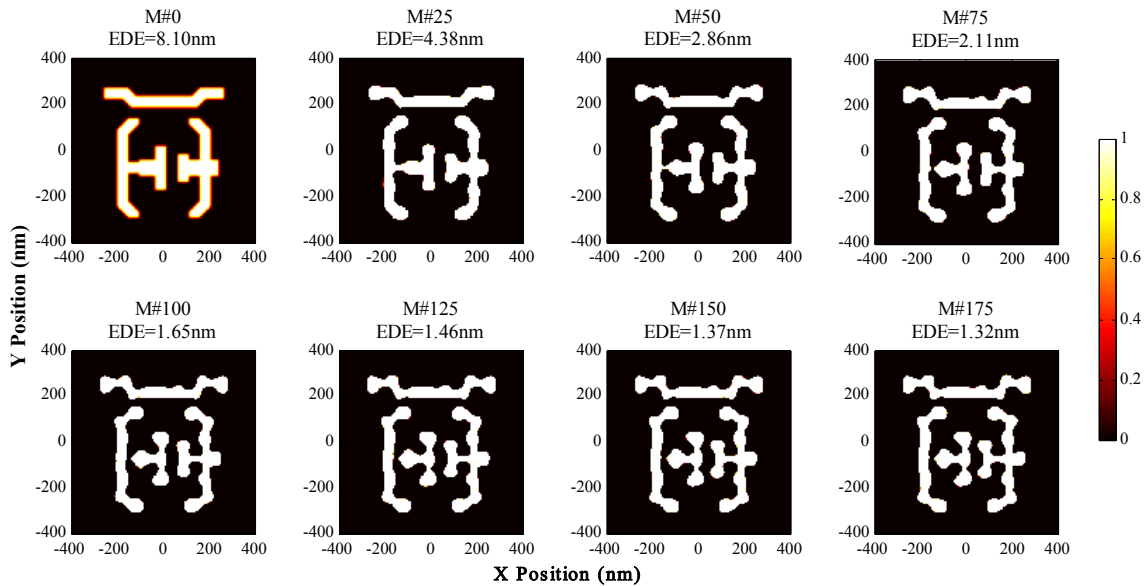


Fig. 5. Some intermediate results obtained in the iteration process by the proposed method.

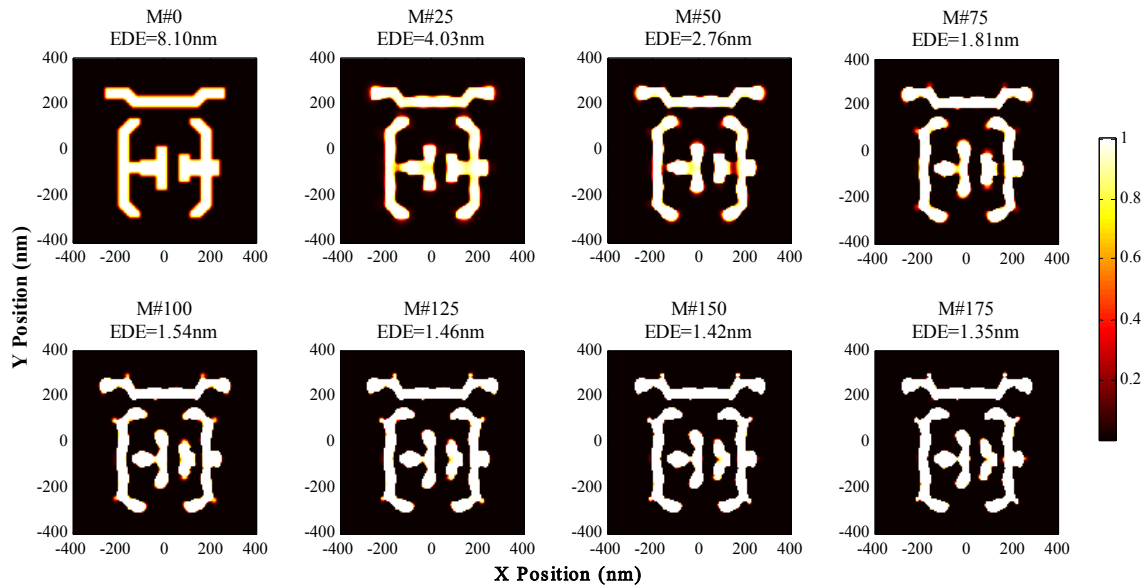


Fig. 6. Some intermediate results obtained in the iteration process by the conventional regularization method.

Figure 7 shows the convergence properties and the solution properties with different methods. From Fig. 7, the results with the conventional regularization method with different weighted parameters λ demonstrate that a small weight causes a fast convergence on EDE but results in a slow convergence on quadratic error; a large weight results in a fast convergence on quadratic error while finally causing a higher EDE. That means a smaller λ will not achieve the

regularization effects, while a larger λ may result in a large EDE. For this reason, it is difficult to choose an appropriate value of weighted parameter λ to get a win-win situation. This is the second drawback of the conventional regularization method. On the other hand, it is observed that the EDE with the proposed method converges rapidly while the quadratic error remains at a low level, which demonstrates that all the intermediate masks satisfy the quadratic error constrains.

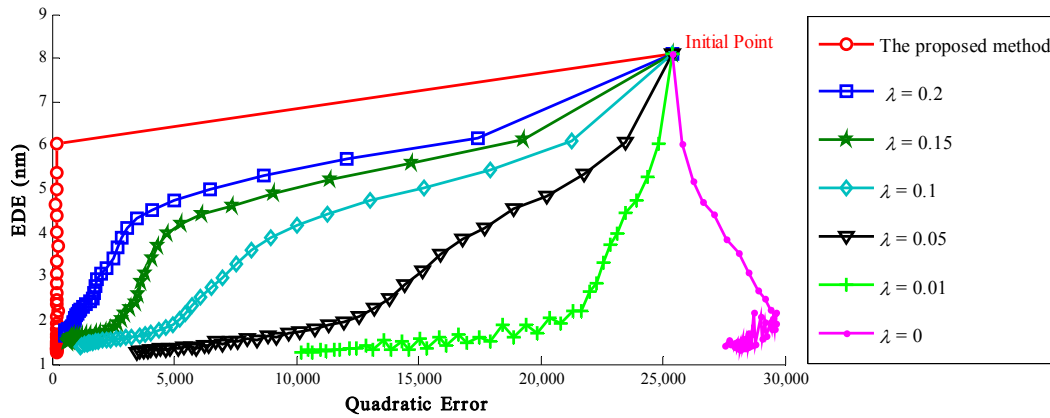


Fig. 7. The convergence properties and solution properties with different methods.

Another two sets of simulation under different illumination conditions are performed and the results are shown in Fig. 8. Simulation of M^1 is performed on a partially coherent imaging system with an annual source illumination ($\sigma_{out}/\sigma_{in} = 0.7/0.4$) and the NA is 0.85. The four images are of size 401×401 pixels with a grid resolution of 2.5 nm. M^{1S} is the mask obtained with the proposed method. Simulation of M^2 is performed on a partially coherent imaging system with a quasar source illumination ($\sigma_{out}/\sigma_{in}/\text{degree} = 0.9/0.6/45^\circ$), and the NA is 1.25. The four images are of size 361×361 pixels with a grid resolution of 2.5 nm. $\Gamma(\cdot)$ is the corresponding resist features. From Fig. 8, it is demonstrated that the proposed method can synthesize a mask pattern under different illumination conditions and shows the possibility of reaching a considerably lower EDE.

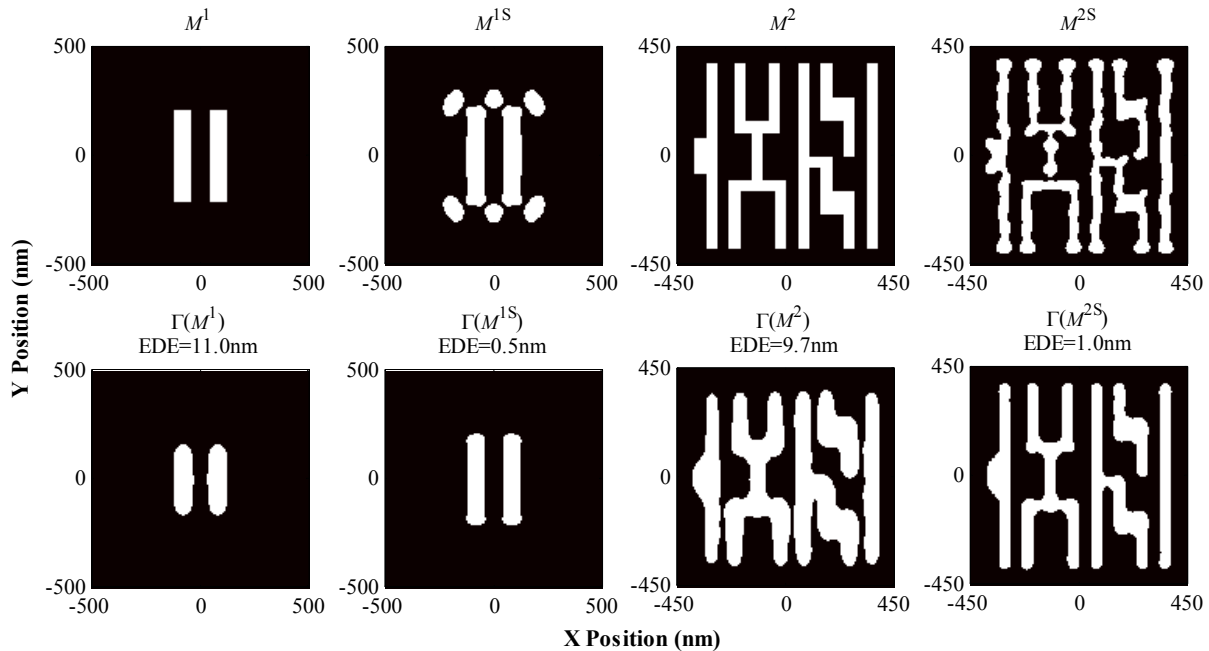


Fig. 8. Some simulation results of the proposed regularization framework. M^1 and M^2 is the target pattern, M^{1S} and M^{2S} is the synthesized mask by the proposed method, and $\Gamma(\cdot)$ represents the corresponding resist feature.

4. CONCLUSIONS

In this paper, we propose a new regularization framework by using a mask filtering technique that regularizes the mask directly to improve computational efficiency and guarantee manufacturability. A tailored mask filter is developed based on the manufacturing constraints. In the proposed regularization framework, each intermediate mask satisfies the manufacturing constraints, so we only need to ensure the decrease of the EDE in the iteration process. In this perspective, the multiple-objective problem is degraded to a single-objective problem. The mask filter is very flexible and can be defined according to different mask manufacturing rules to make a filtered mask that can be sent directly to fabrication. Compared to the conventional regularization method, the proposed method avoids choosing weighted parameters of various regularization terms and guarantees the manufacturability of each intermediate mask without raising computational complexity. In addition, we develop a new metric, EDE, which has the same dimension nanometer as EPE and has a continuous expression as pattern error, to guide mask synthesis. Simulation demonstrated the validity and efficiency of the proposed method.

ACKNOWLEDGMENT

This work was funded by the National Natural Science Foundation of China (Grant No. 91023032, 51005091, 51121002), the Specialized Research Fund for the Doctoral Program of Higher Education of China (Grant No. 20120142110019), the National Science and Technology Major Project of China (Grant No. 2012ZX02701001), and the National Instrument Development Specific Project of China (Grant No. 2011YQ160002).

REFERENCES

- [1] A. K. Wong, *Resolution Enhancement Techniques in Optical Lithography* (SPIE Press, 2001).
- [2] F. Schellenberg, "Resolution enhancement technology: the past, the present, and extensions for the future," Proc. SPIE **5377**, 1–20 (2004).
- [3] A. Poonawala and P. Milanfar, "Mask design for optical microlithography - an inverse imaging problem," IEEE Trans. Image Process. **16**(3), 774–788 (2007).
- [4] S. Y. Liu, "Computational lithography and computational metrology for nanomanufacturing," Proceedings of the 6th IEEE International Conference on Nano/Micro Engineered and Molecular Systems, 1093-1099 (Invited paper, 2011).
- [5] X. Ma and G. R. Arce, "Pixel-based OPC optimization based on conjugate gradients," Opt. Express **19**(3), 2165–2180 (2011).
- [6] Y. Granik, "Fast pixel-based mask optimization for inverse lithography," J. Micro/Nanolith. MEMS MOEMS. **5**(4): 043002 (2006).
- [7] N. B. Cobb and Y. Granik, "Using OPC to optimize for image slope and improve process window". Proc. SPIE **5130**, 838-846 (2003).
- [8] Y. Granik and N. B. Cobb, "MEEF as a matrix," Proc. SPIE **4562**, 980-991 (2002).
- [9] B. Bourdin, "Filters in topology optimization," International Journal for Numerical Methods in Engineering **50**, 2143–2158 (2001).
- [10] M. P. Bendsøe and O. Sigmund, *Topology Optimization: Theory, Methods and Applications*, (Springer, 2003).
- [11] N. B. Cobb, "Fast optical and process proximity correction algorithms for integrated circuit manufacturing," Ph.D. Dissertation (University of California at Berkeley, 1998).
- [12] P. Yu, S. X. Shi, and D. Z. Pan, "True process variation aware optical proximity correction with variational lithography modeling and model calibration," J. Micro/Nanolith. MEMS MOEMS. **6**: 031004 (2007).
- [13] N. Jia, A. K. Wong, and E. Y. Lam, "Robust mask design with defocus variation using inverse synthesis," in Proc. SPIE **7140**: 71401W (2008).
- [14] S. Choy, N. Jia, C. Tong, M. Tang, and E. Y. Lam, "A robust computational algorithm for inverse photomask synthesis in optical projection lithography," SIAM J. Imaging Sciences **5**(2), 625-651 (2012).
- [15] A. K. Wong, *Optical Imaging in Projection Microlithography* (SPIE Press, 2005).
- [16] Y. C. Pati and T. Kailath, "Phase-shifting masks for microlithography: automated design and mask requirements," J. Opt. Soc. Am. A **11**(9), 2438–2452 (1994).
- [17] P. Gong, S. Y. Liu, W. Lv, and X. J. Zhou, "Fast aerial image simulations for partially coherent systems by transmission cross coefficient decomposition with analytical kernels," J. Vac. Sci. Technol. B **30**(6): 06FG03 (2012).